26

Visual Control System for Robotic Welding

De Xu, Min Tan and Yuan Li

1. Introduction

In general, the teaching by showing or offline programming is used for path planning and motion programming for the manipulators. The actions preset are merely repeated in the working process. If the states of work piece varied, the manufacture quality would be influenced too intensely to satisfy the demand of production. In addition, the teaching by showing or offline programming costs much time, especially in the situations that much manufacture variety with little amount. The introduction of visual measurement in robot manufacture system could eliminate the teaching time and ensure the quality even if the state of the work piece were changed. Obviously, visual control can make the robot manufacture system have higher efficiency and better results (Bolmsjo et al., 2002; Wilson, 2002).There are many aspects concerned with the visual control for robotic welding such as vision sensor, image processing, and visual control method.As a kind of contactless seam detecting sensors, structured light vision sensor plays an important role in welding seam tracking. It has two categories. One uses structured light to form a stripe, and the other uses laser scanning. Structured light vision is regarded as one of the most promising methods because of its simplicity, higher accuracy and good performance in real-time (Wu & Chen, 2000). Many researchers pay their attention to it (Bakos et al., 1993; Zou et al., 1995; Haug & Pristrchow, 1998; Zhang & Djordjevich, 1999; Zhu & Qiang, 2000; Xu et al., 2004). For example, Bakos established a structured light measurement system, which measurement precision is 0.1mm when the distance is 500 mm. Meta Company provides many kinds of laser structured light sensors. In general, the sensor should be calibrated before putting into action. Camera calibration is an important classic topic, and a lot of literatures about it can be found (Faugeras & Toscani, 1986; Tsai, 1987; Ma, 1996; Zhang, 2000). But the procedure is complicated and tedious, especially that of the laser plane's calibration (Zhang & Djordjevich, 1999). Another problem in structured light vision is the difficulty of image processing. The structured light image of welding seam is greatly affected by strong arc light, smog and splash in the process of arc welding (Wu & Chen, 2000). Not only the image is rough, but also its background is noisy. These give rise

Source: Industrial-Robotics-Theory-Modelling-Control, ISBN 3-86611-285-8, pp. 964, ARS/plV, Germany, December 2006, Edited by: Sam Cubero

to difficulty, error and even failure of the processing of the welding seam image. Intelligent recognition algorithms, such as discussed in (Kim et al., 1996; Wu et al., 1996), can effectively eliminate some of the effects. However, besides intelligent recognition algorithm, it is an effective way for the improvement of recognition correctness to increase the performance of image processing.

The visual control methods fall into three categories: position-based, image-based and hybrid method (Hager et al., 1996; Corke & Good, 1996; Chaumette & Malis, 2000). As early as 1994, Yoshimi and Allen gave a system to find and locate the object with "active uncalibrated visual servoing" (Yoshimi & Allen, 1994). Experimental results by Cervera et al. demonstrated that using pixel coordinates is disadvantageous, compared with 3D coordinates estimated from the same pixel data (Cervera et al., 2002). On the other hand, although position-based visual control method such as (Corke & Good, 1993; 1996) has better stableness, it has lower accuracy than former because the errors of kinematics and camera have influence on its precision. Malis et al. proposed hybrid method that controls the translation in image space and rotation in Cartesian space. It has the advantages of two methods above (Malis et al., 1998; 1999; Chaumette & Malis, 2000).

In this chapter, a calibration method for the laser plane is presented, which is easy to be realized and provides the possibility to run hand-eye system calibration automatically. Second, the image processing methods for the laser stripe of welding seam are investigated. Third, a novel hybrid visual servoing control method is proposed for robotic arc welding with a general six degrees of freedom robot.The rest of this chapter is arranged as follows. The principle of a structured light vision sensor is introduced in Section 2. And the robot frames are also assigned in this Section. In Section 3, the laser plane equation of a structured light visual sensor is deduced from a group of rotation, in which the position of the camera's optical centre is kept unchangeable in the world frame. In Section 4, a method to extract feature points based on second order difference is proposed for type V welding seams. A main characteristic line is obtained using Hotelling transform and Hough transform. The feature points in the seam are found according to its second difference. To overcome the reflex problem, an improved method based on geometric centre is presented for multi-pass welding seams in Section 5. The profiles of welding seam grooves are obtained according to the column intensity distribution of the laser stripe image. A gravity centre detection method is provided to extract feature points on the basis of conventional corner detection method. In Section 6, a new hybrid visual control method is concerned. It consists of a position control inner loop in Cartesian space and two outer loops. One outer loop is position-based visual control in Cartesian space for moving in the direction of the welding seam, i.e. welding seam tracking; another is image-based visual control in image space for adjustment to eliminate the errors in tracking. Finally, this chapter is ended with conclusions in Section 7.

2. Structured light vision sensor and robot frame

2.1 Structured light vision sensor

The principle of visual measurement with structured light is shown in Fig. 1. A lens shaped plano-convex cylinder is employed to convert a laser beam to a plane, in order to form a stripe on the welding works. A CCD camera with a light filter is used to capture the stripe. It is a narrow band filter to allow the light in a small range with the centre of laser light wavelength to pass through. It makes the laser stripe image be very clear against the dark background. A laser emitter, a plano-convex cylinder lens, and a camera with a light filter constitute a structured light vision sensor, which is mounted on the end-effector of an arc welding robot to form a hand-eye system. The camera outputs a video signal, which is input to an image capture card installed in a computer. Then the signal is converted to image (Xu et al., 2004a).

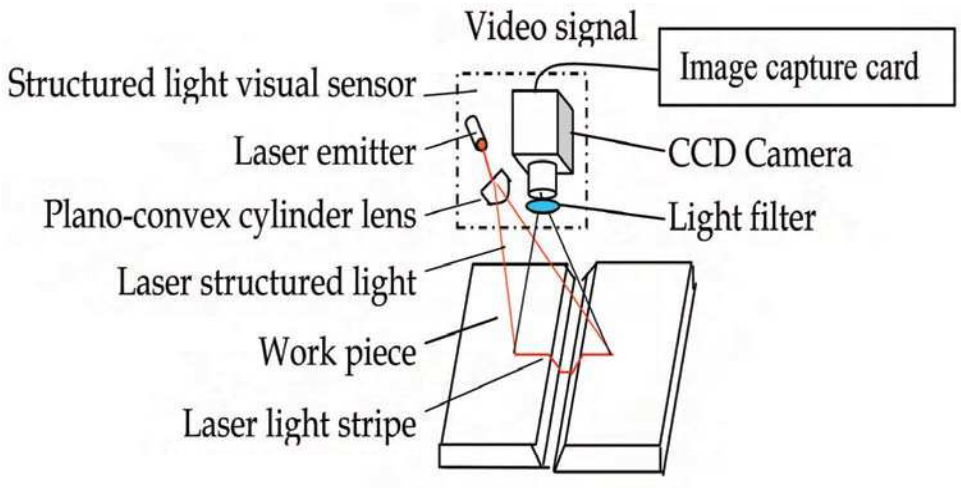

Figure 1. The principle of structured light vision sensor

2.2 Robot frame assignment

Coordinates frames are established as shown in Fig. 2. Frame *W* represents the original coordinates, i.e. the world frame. Frame *E* the end-effector coordinates. Frame *R* the working reference coordinates. Frame *C* the camera coordinates. The camera frame *C* is established as follows. Its origin is assigned at the optical centre of the camera. Its *z*-axis is selected to the direction of the optical axis from the camera to the scene. Its *x*-axis is selected as horizontal direction of its imaging plane from left to right. ${}^{w}T_{r}$ indicates the transformation from

frame W to R, i.e. the position and orientation of frame R expressed in frame W. And ${}^{r}T_{c}$ is from frame R to C, ${}^{w}T_{e}$ from frame W to E, ${}^{e}T_{c}$ from frame E to C.

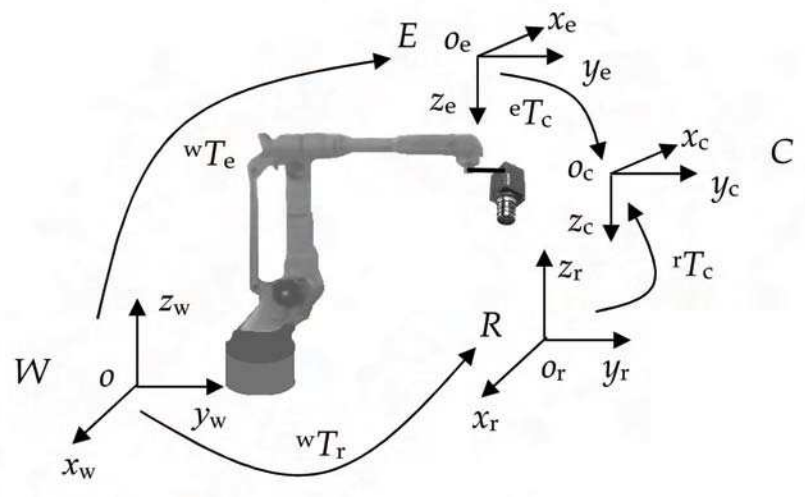

Figure 2. The sketch figure of coordinates and transformation

3. Laser plane calibration

3.1 Calibration method based on rotation

Generally, the camera is with small view angle, and its intrinsic parameters can be described with pinhole model, as given in (1). Its extrinsic parameters can be given in (2).

$$\begin{bmatrix} u \\ v \\ 1 \end{bmatrix} = \begin{bmatrix} k_x & 0 & u_0 \\ 0 & k_y & v_0 \\ 0 & 0 & 1 \end{bmatrix} \begin{bmatrix} x_c / z_c \\ y_c / z_c \\ 1 \end{bmatrix} = M_{in} \begin{bmatrix} x_c / z_c \\ y_c / z_c \\ 1 \end{bmatrix} \tag{1}$$

where $[u, v]$ are the coordinates of a point in an image, $[u_0, v_0]$ denote the image coordinates of the camera's principal point, $[x_c, y_c, z_c]$ are the coordinates of a point in the camera frame, M_{in} is the intrinsic parameters matrix, and $[k_x, k_y]$ are the magnification coefficients from the imaging plane coordinates to the image coordinates. In fact, $[k_x, k_y]$ are formed with the focal length and the magnification factor from the image size in mm to the imaging coordinates in pixels.

$$\begin{bmatrix} x_c \\ y_c \\ z_c \end{bmatrix} = \begin{bmatrix} n_x & o_x & a_x & p_x \\ n_y & o_y & a_y & p_y \\ n_z & o_z & a_z & p_z \end{bmatrix} \begin{bmatrix} x_w \\ y_w \\ z_w \\ 1 \end{bmatrix} = {}^{c}M_w \begin{bmatrix} x_w \\ y_w \\ z_w \\ 1 \end{bmatrix} \tag{2}$$

where $[x_w, y_w, z_w]$ are the coordinates of a point in the object frame, and ${}^{c}M_w$ is the extrinsic parameter matrix of the camera, i.e. the transformation from the camera frame *C* to the world frame *W*. In ${}^{c}M_w$, $\vec{n} = [n_x \quad n_y \quad n_z]^T$ is the direction vector of the *x*-axis, $\vec{o} = [o_x \quad o_y \quad o_z]^T$ is that of the *y*-axis, $\vec{a} = [a_x \quad a_y \quad a_z]^T$ is that of the *z*-axis for the frame *W* expressed in the frame *C*, and $\vec{p} = [p_x \quad p_y \quad p_z]^T$ is the position vector.

Camera calibration is not a big problem today. But laser plane calibration is still difficult. Therefore, the calibration of structured light vision sensor is focused on laser plane except camera. In the following discussion (Xu & Tan, 2004), the parameters of a camera are supposed to be well calibrated in advance.

Assume the equation of the laser light plane in frame *C* is as follows

$$ax + by + cz + 1 = 0 \tag{3}$$

where *a*, *b*, *c* are the parameters of the laser light plane.

An arbitrary point *P* in laser stripe must be in the line formed by the lens centre and the imaging point $[x_{c1}, y_{c1}, 1]$. Formula (4) shows the equation of the line in frame *C*.

$$[x \quad y \quad z]^T = [x_{c1} \quad y_{c1} \quad 1]^T t \tag{4}$$

where $x_{c1}=x_c/z_c$, $y_{c1}=y_c/z_c$, *t* is an intermediate variable.

On the other hand, the imaging point $[x_{c1}, y_{c1}, 1]^T$ can be calculated from (1) as follows.

$$[x_{c1} \quad y_{c1} \quad 1]^T = M_{in}^{-1} [u \quad v \quad 1]^T \tag{5}$$

From (3) and (4), the coordinates of point *P* in frame *C* can be expressed as the functions of parameter *a*, *b*, and *c*, given in (6). Further more, its coordinates $[x_w, y_w, z_w]$ in frame *W* can be had as given in (7).

$$\begin{cases} x = -x_{c1} / (ax_{c1} + by_{c1} + c) \\ y = -y_{c1} / (ax_{c1} + by_{c1} + c) \\ z = -1 / (ax_{c1} + by_{c1} + c) \end{cases} \tag{6}$$

$$\begin{bmatrix} x_w & y_w & z_w & 1 \end{bmatrix}^T = {}^wT_e \, {}^eT_c \begin{bmatrix} x & y & z & 1 \end{bmatrix}^T \tag{7}$$

Let

$${}^wT_e \, {}^eT_c = \begin{bmatrix} n_x & o_x & a_x & p_x \\ n_y & o_y & a_y & p_y \\ n_z & o_z & a_z & p_z \\ 0 & 0 & 0 & 1 \end{bmatrix} = \begin{bmatrix} \vec{n} & \vec{o} & \vec{a} & \vec{p} \\ 0 & 0 & 0 & 1 \end{bmatrix} \tag{8}$$

then (9) is deduced from (7) and (8).

$$\begin{cases} x_w = n_x x + o_x y + a_x z + p_x \\ y_w = n_y x + o_y y + a_y z + p_y \\ z_w = n_z x + o_z y + a_z z + p_z \end{cases} \tag{9}$$

If the surface of work piece is a plane, the points in the laser stripe will satisfy its plane equation (10).

$$Ax_w + By_w + Cz_w + 1 = 0 \tag{10}$$

in which A, B and C are the parameters of the work piece plane in frame W. Submitting (9) to (10), then

$$\begin{aligned} &A(n_x x + o_x y + a_x z) + B(n_y x + o_y y + a_y z) + \\ &C(n_z x + o_z y + a_z z) + Ap_x + Bp_y + Cp_z + 1 = 0 \end{aligned} \tag{11}$$

Let $D=Ap_x+Bp_y+Cp_z+1$. It is sure that the lens centre of the camera, $[p_x, p_y, p_z]$, is not on the plane of work piece. Therefore the condition $D \neq 0$ is satisfied. Equation (11) is rewritten as (12) via divided by D and applying (6) to it (Xu & Tan, 2004).

$$\begin{aligned} &A_1(n_x x_{c1} + o_x y_{c1} + a_x) + B_1(n_y x_{c1} + o_y y_{c1} + a_y) \\ &+C_1(n_z x_{c1} + o_z y_{c1} + a_z) - ax_{c1} - by_{c1} - c = 0 \end{aligned} \tag{12}$$

here $A_1=A/D$, $B_1=B/D$, $C_1=C/D$.

If the optical axis of the camera is not parallel to the plane of the laser light, then $c \neq 0$ is satisfied. In fact, the camera must be fixed in some direction except that parallel to the plane of the laser light in order to capture the laser stripe. Dividing (12) by c, then

$$\begin{aligned} &A_2(n_x x_{c1} + o_x y_{c1} + a_x) + B_2(n_y x_{c1} + o_y y_{c1} + a_y) \\ &+C_2(n_z x_{c1} + o_z y_{c1} + a_z) - a_1 x_{c1} - b_1 y_{c1} = 1 \end{aligned} \tag{13}$$

where $A_2=A_1/c$, $B_2=B_1/c$, $C_2=C_1/c$, $a_1=a/c$, $b_1=b/c$.

In the condition that the point of the lens centre $[p_x, p_y, p_z]$ is kept unchangeable in frame O, a series of laser stripes in different directions are formed with the pose change of the vision sensor. Any point in each laser stripe on the same plane of a work piece satisfies (13). Notice the linear correlation, only two points can be selected from each stripe to submit to formula (13). They would form a group of linear equations, whose number is as two times as that of stripes. If the number of equations is greater than 5, they can be solved with least mean square method to get parameters such as A_2, B_2, C_2, a_1, b_1.
Now the task of laser calibration is to find the parameter c. The procedure is very simple. It is well known that the distance between two points P_i and P_j on the stripe is as follows

$$d = \sqrt{(x_{wi} - x_{wj})^2 + (y_{wi} - y_{wj})^2 + (z_{wi} - z_{wj})^2} = \sqrt{d_x^2 + d_y^2 + d_z^2} \tag{14}$$

in which, $[x_{wi}, y_{wi}, z_{wi}]$ and $[x_{wj}, y_{wj}, z_{wj}]$ are the coordinates of point P_i and P_j in the world frame; d_x, d_y, d_z are coordinates decomposition values of distance d. Submitting (6) and (9) to (14), then

$$\begin{aligned} d_x = \frac{1}{c}[& n_x\left(\frac{x_{c1j}}{a_1 x_{c1j} + b_1 y_{c1j} + 1} - \frac{x_{c1i}}{a_1 x_{c1i} + b_1 y_{c1i} + 1}\right) \\ & + o_x\left(\frac{y_{c1j}}{a_1 x_{c1j} + b_1 y_{c1j} + 1} - \frac{y_{c1i}}{a_1 x_{c1i} + b_1 y_{c1i} + 1}\right) \\ & + a_x\left(\frac{1}{a_1 x_{c1j} + b_1 y_{c1j} + 1} - \frac{1}{a_1 x_{c1i} + b_1 y_{c1i} + 1}\right)] = \frac{1}{c} d_{x1} \end{aligned} \tag{15}$$

In the same way, d_y and d_z are deduced. Then

$$d = \pm\frac{1}{c}\sqrt{d_{x1}^2 + d_{y1}^2 + d_{z1}^2} = \pm\frac{1}{c} d_1 \Rightarrow c = \pm\frac{d_1}{d} \tag{16}$$

where d_1 is the calculated distance between two points on the stripe with parameters a_1 and b_1, and d is the measured distance with ruler.
Then parameters a and b can be directly calculated from c as formula (17). Applying a, b, and c to (6), the sign of parameter c could be determined with the constraint z>0.

$$\begin{cases} a = a_1 c \\ b = b_1 c \end{cases} \tag{17}$$

3.2 Experiment and results

The camera in the vision sensor was well calibrated in advance. Its intrinsic parameters M_{in} and extrinsic ones ${}^{\text{e}}T_{\text{c}}$ were given as follows.

$$M_{in} = \begin{bmatrix} 2620.5 & 0 & 408.4 \\ 0 & 2619.1 & 312.2 \\ 0 & 0 & 1 \end{bmatrix}, \quad {}^{e}T_{c} = \begin{bmatrix} -0.0867 & -0.6620 & -0.7444 & 51.9160 \\ -0.0702 & 0.7495 & -0.6583 & -89.9243 \\ 0.9938 & -0.0048 & -0.1115 & 35.3765 \\ 0 & 0 & 0 & 1 \end{bmatrix}.$$

in which the image size is 768×576 pixels.

3.2.1 Laser Plane Calibration

A structured light vision sensor was mounted on the end-effector of an arc welding robot to form a hand-eye system. The laser stripe was projected to a plane approximately parallel to the XOY plane in frame W. The poses of the vision sensor were changed through the end-effector of the robot for seven times. And the lens centre point [p_x, p_y, p_z] was kept unchangeable in frame W in this procedure. So there were seven stripes in different directions. Any two points were selected from each stripe to submit to (13). Fourteen linear equations were formed. Then the parameters such as A_2, B_2, C_2, a_1, b_1 could be obtained from them. It was easy to calculate the length d_1 of one stripe with a_1 and b_1, and to measure its actual length d with a ruler. In fact, any two points on a laser stripe satisfy (14)-(16) whether the laser stripe is on a plane or not. To improve the precision of manual measure, a block with known height was employed to form a laser stripe with apparent break points, as seen in Fig. 3. The length d_1 was computed from the two break points. Then parameters of the laser plane equation were directly calculated with (13)-(17). The results are as follows.

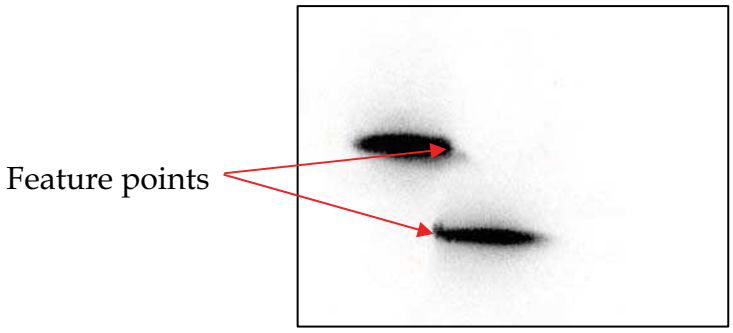

Figure 3. A laser stripe formed with a block

d=23mm, d_1=0.1725, a=-9.2901×10^{-4}, b=2.4430×10^{-2}, c=-7.5021×10^{-3}.

So the laser plane equation in frame C is:
-9.2901×10^{-4}x+2.4430×10^{-2}y-7.5021×10^{-3}z+1=0.

3.2.2 The verification of the hand-eye system

A welding seam of type V was measured by use of the structured light vision sensor to verify the hand-eye system. The measurements were conducted 15 times along the seam. Three points were selected from the laser stripe for each time, which were two edge points and a bottom one. Their coordinates in frame W were computed via the method proposed above. The results were shown in Table 1.

No.	1	2	3	4	5	6	7	8	9	10	11	12	13	14	15
x_{w1}	1019.16	1007.22	1003.34	999.55	991.11	983.95	977.16	973.85	971.13	967.05	963.89	959.34	954.90	952.73	946.64
y_{w1}	38.68	72.51	82.53	93.17	116.12	136.33	153.67	163.10	171.24	182.04	190.31	202.58	214.91	220.74	236.73
z_{w1}	47.09	46.70	46.85	46.66	46.74	46.50	46.74	46.93	46.74	46.68	46.73	46.85	46.73	46.57	46.74
x_{w2}	1031.54	1019.68	1016.36	1012.30	1004.21	996.99	990.81	987.51	984.34	980.33	977.27	972.92	968.07	965.91	960.26
y_{w2}	24.70	57.74	67.19	78.23	100.78	120.92	137.80	147.07	155.73	166.29	174.60	186.46	199.29	205.46	221.04
z_{w2}	37.41	36.58	36.32	36.39	36.20	35.93	35.81	35.91	36.09	35.89	35.94	35.80	36.02	36.05	35.93
x_{w3}	1031.10	1019.13	1015.84	1011.80	1003.76	996.31	989.97	986.84	983.85	979.87	976.71	971.97	967.45	965.37	959.34
y_{w3}	43.27	76.36	86.24	96.94	120.13	140.46	156.70	166.41	174.89	185.57	194.14	206.13	218.65	225.10	241.18
z_{w3}	47.53	46.75	46.71	46.61	46.74	46.62	46.18	46.49	46.54	46.40	46.61	46.60	46.60	46.76	46.98

Table 1. The measurement results of a welding seam of type V

Row 1 was the sequence number of measurement points. Row 2 was one of outside edges of the seam. Row 4 was another. Row 3 was its bottom edge. All data were with unit mm in the world frame. The measurement errors were in the range ±0.2mm. The measurement results are also shown in the world frame and XOY plane in Fig. 4 respectively. Fig. 4 is the data graph shown in 3D space, and Fig. 4 on XOY plane in frame W. It can be seen that the results were well coincided with the edge lines of the seam (Xu & Tan, 2004).

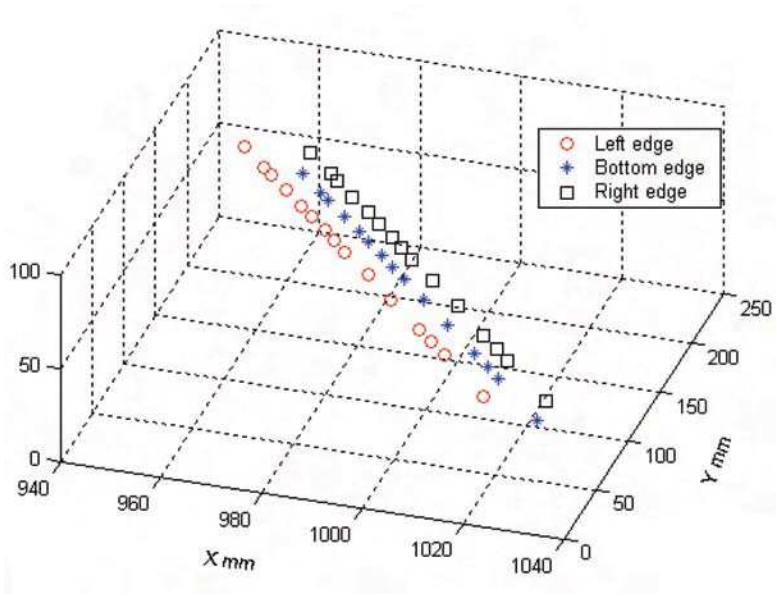

(a) 3D space

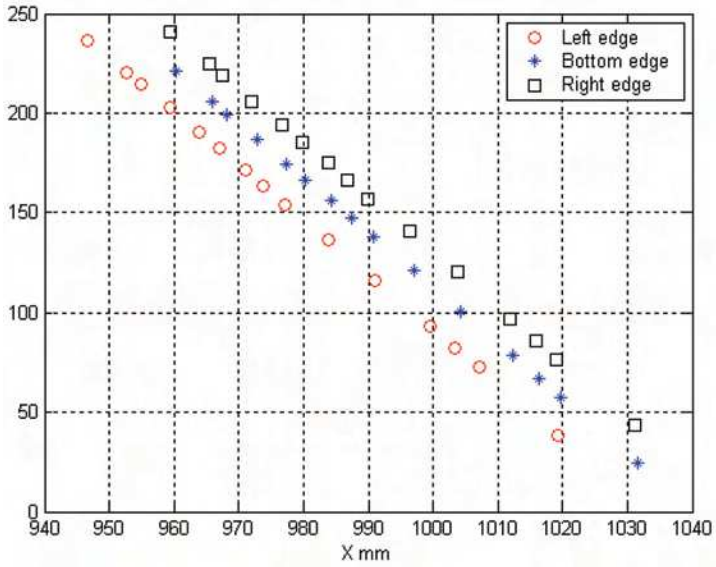

(b) XOY plane

Figure 4. The data graph of vision measurement results of a type V welding seam

4. Feature extraction based on second order difference

4.1 Image pre-processing

The gray image of laser stripe is captured via a camera with light filter. Generally, its size is large. For example, it could be as large as 576×768 pixels. Therefore, simple and efficient image pre-processing is essential to improve visual control performance in real time. The image pre-processing includes image segmentation, image enhancement and binarization (Xu et al., 2004a; 2004b).

4.1.1 Image segmentation

First, the background gray value of the image is counted. Along its horizontal and perpendicular direction, lines with constant space are drawn. Gray values of all pixels on the lines are added, and its average value is taken as the gray value of background. It is given in (18).

$$\begin{cases} B = \dfrac{1}{n_w n_1 + n_h n_2}\left(\sum\limits_{i=1}^{n_w}\sum\limits_{j=1}^{n_1} I(i,10j) + \sum\limits_{i=1}^{n_2}\sum\limits_{j=1}^{n_h} I(10i,j) \right) \\ n_1 = Int(n_h/10),\ n_2 = Int(n_w/10) \end{cases} \tag{18}$$

where n_w and n_h are the image width and height respectively, n_1 is the number of horizontal lines, n_2 is the number of vertical lines, and $I(x, y)$ is the gray value of the pixel in coordinates (x, y).

Usually, laser stripe has higher brightness than the background. Along the lines drawn above, all pixels with gray value greater than $B+T_1$ are recorded. The target area on the image is confirmed according to the maximum and the minimum coordinates of pixels recorded along the horizontal and perpendicular direction respectively.

$$\begin{cases} X_1 = Min\{i : I(i,10j_1) - B > T_1 \text{ or } I(10i_1, j) - B > T_1\} \\ X_2 = Max\{i : I(i,10j_1) - B > T_1 \text{ or } I(10i_1, j) - B > T_1\} \\ Y_1 = Min\{j : I(i,10j_1) - B > T_1 \text{ or } I(10i_1, j) - B > T_1\} \\ Y_2 = Max\{j : I(i,10j_1) - B > T_1 \text{ or } I(10i_1, j) - B > T_1\} \\ 1 \le i \le n_w, 1 \le j \le n_h, i_1 = INT(i/10), j_1 = INT(j/10) \end{cases} \tag{19}$$

where T_1 is the gray threshold. The target area consists of X_1, X_2, Y_1 and Y_2.

The structured light image is suffered from arc light, splash, and acutely changed background brightness during welding. As known, the intensity of the arc light and splash changes rapidly, but the laser intensity keeps stable. According to this fact, the effect of arc light and splash can be partly eliminated via taking the least gray value between sequent images as the new gray

value of the image.

$$I(i,j) = Min\{I_k(i,j), I_{k-1}(i,j)\} \tag{20}$$

where I_k is the image captured at k-th times, and I_{k-1} is k-1-th. $X_1 \le i \le X_2$, $Y_1 \le j \le Y_2$.

4.1.2 Image enhancement and binarization

The target area is divided into several parts, and its gray values are divided into 25 levels. For every part, the appearance frequency of every gray level is calculated, as given in (21).

$$\begin{cases} F(k,h) = \sum_{i=X_1}^{X_2} \sum_{j=Y_1}^{Y_2} P(k,h) \\ P(k,h) = \begin{cases} 1 & k = Int(i/5), h = Int(I(i,j)/10) \\ 0 & others \end{cases} \end{cases} \tag{21}$$

Taking into account the different contrast between the laser stripe and background, the gray value with higher level, whose appearance reaches specified frequency, is regarded as the image enhancement threshold $T_2(k)$.

$$T_2(k) = 10K, iff\ (\sum_{h=25}^{K} F(k,h) > S_1) \vee (F(k,K) > S_2) \tag{22}$$

where S_1 is the specified sum of the frequency with the higher gray level, S_2 is the specified frequency with higher level in one child area, and K is the gray level, $1 \le K \le 25$.

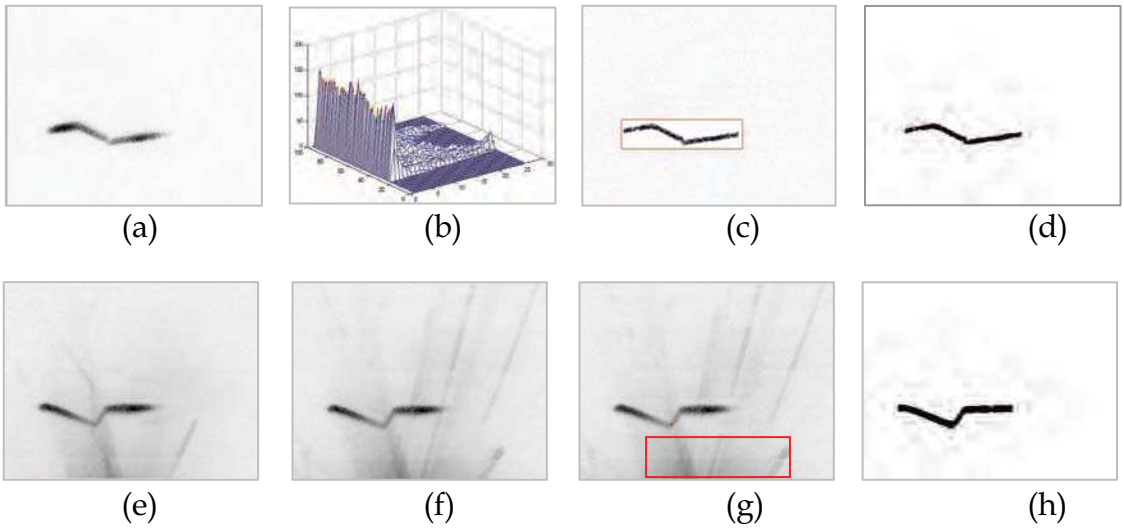

Figure 5. The primary image, frequency distribution map and object segmentation

According to the threshold of every child area, high-pass filter and image enhancement are applied to the target area, followed by Gauss filter and binary thresholding. Fig. 5 is the result of image segmentation of a welding seam. In detail, Fig. 5(a) is the original image with inverse colour, Fig. 5(b) shows its distribution of gray frequency, Fig. 5(c) is the image of the strengthened target area, and Fig. 5(d) is the binary image. Fig. 5(e) and Fig. 5(f) are two frames of original images with inverse colour in sequence during welding, and Fig. 5(g) is the processing result via taking the least gray value in the target area with (20). Fig. 5(h) is its binary image. It can be seen that the binary images of welding seams, obtained after image pre-processing with the proposed method, are satisfactory.

4.2 Features extraction

Because the turning points of the laser stripe are the brim points of the welding seam, they are selected as the feature points. To adjust the pose of the weld torch easily, some points on the weld plane are required. Therefore, the goal of features extraction is to search such turning points and weld plane points from the binary image.

To thin the binary image of welding seam, the average location between the upper edge and the lower one, which is detected from the binary image, is regarded as the middle line of laser stripe. Fig. 6(a) shows the upper, lower edge, and middle line of the laser stripe. Because of the roughness of the binary laser stripe, the middle line curve has noise with high frequency, seen in the bottom of Fig. 6(b).

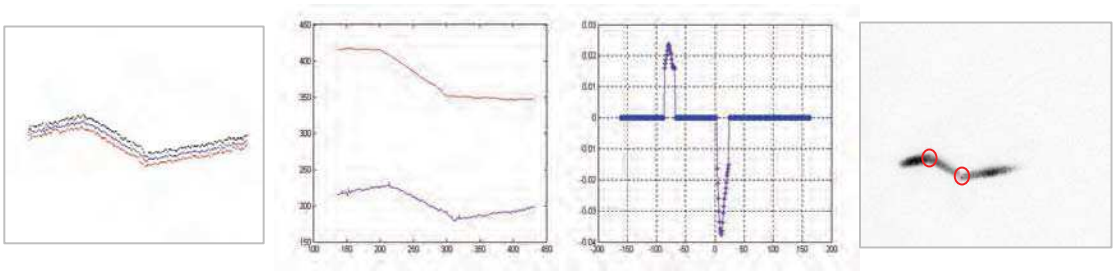

(a) (b) (c) (d)

Figure 6. The procedure of features extraction

The middle line stored in an array with two dimensions is transformed via Hotelling transformation, to make its feature direction same as the x-axis. Hotelling transformation is shortly described as follows.

First, the position vector of the average of all points on the middle line is computed.

$$\overline{m}_d = \frac{1}{N}\sum_{i=1}^{N} m_d(i) \tag{23}$$

where N is the point number on the middle line, and $\overline{m}_d$ is the position vector of the average, $\overline{m}_d = [\overline{m}_d(1) \quad \overline{m}_d(2)]^T$. $m_d(i,1)$ is the coordinate x of the i-th point, and $m_d(i,2)$ is the coordinate y.

Second, the position vector of each point on the middle line after Hotelling transformation is calculated.

$$C_d = \frac{1}{N}\sum_{i=1}^{N} m_d(i) m_d(i)^T - \overline{m}_d \overline{m}_d{}^T \tag{24}$$

$$m_{dh}(i) = V[m_d(i) - \overline{m}_d] \tag{25}$$

where $m_{dh}(i) = [m_{dh}(i,1) \quad m_{dh}(i,2)]^T$ is the position vector of the i-th point on the middle line after Hotelling transformation. V is the eigenvector matrix of C_d, whose first row has large eigenvalue.

To clear up the effect of high frequency noise, the middle line after Hotelling transformation should be filtered. In the condition to keep the x-coordinate invariable, y-coordinate is filtered using Takagi-Sugeno fuzzy algorithm, given by equation (26) and (27).

$$\tilde{m}_{dh}(k,2) = [\sum_{h=-5}^{5} m_{dh}(k-h,2)\mu(h)] \Big/ \sum_{h=-5}^{5} \mu(h) \tag{26}$$

where $\tilde{m}_{dh}(k,2)$ is the y-coordinate of the k-th point on the filtered middle line. $\mu(h)$ is the membership function.

$$\mu(h) = \begin{cases} 1 & -3 \le h \le 3 \\ 2 - |h|/3 & 3 < |h| \le 5 \\ 0 & |h| > 5 \end{cases} \tag{27}$$

A line gained by Hough transform, which is the closest to the x-axis direction converted by Hotelling transformation, is viewed as the main line. Locations of points on the middle line are mapped into the parameter space $A(p, q)$ of the line function, shown in (28), and the (p, q) with the maximum value of A is the

parameter of the main line. All points on the middle line satisfied with the main line function are feature points of the weld plane.

$$\begin{cases} A(p,q)=\sum_{k=1}^{M}\sum_{p=pMin}^{pMax}B(p,q) \\ B(p,q)=\begin{cases}1 & q=-p\tilde{m}_{dh}(k,1)+\tilde{m}_{dh}(k,2) \\ 0 & others\end{cases}\end{cases} \tag{28}$$

The main line is rotated an angle in order to make it parallel to the x-axis direction.

$$m_{dr}(i)=V_1\tilde{m}_{dh}(i)=\begin{bmatrix}\cos\theta & -\sin\theta \\ \sin\theta & \cos\theta\end{bmatrix}\tilde{m}_{dh}(i) \tag{29}$$

where θ=atan(p) is the inclination angle between the main line and x-axis, $m_{dr}(i)$ is the position vector of the i-th point on the rotated middle line, V_1 is a rotation matrix formed with $\cos\theta$ and $\sin\theta$.

The point with the maximum of the local second derivative is the turning point of the middle line. After reverse transform as given in (30), the position of the welding seam feature point in the original image is obtained.

$$m_{dm}(i)=V^{-1}V_1^{-1}m_{drm}(i)+\overline{m}_d \tag{30}$$

where $m_{drm}(i)$ is the position vector of the i-th turning point on the middle line, and $m_{dm}(i)$ is the turning point position in the original image.

The curve at the top of Fig. 6(b) shows the middle line after filtered and transformed. The second derivative of the middle line is seen in Fig. 6(c). Two feature points of the welding seam on the original image can be read from Fig. 6(d).

5. Feature extraction based on geometric centre

5.1 Algorithms for profiles extraction

Fig. 7 shows two frames of laser images of a welding seam of type V groove, in which Fig. 7(a) is an original image before welding, and Fig. 7(b) is an image with reflection of laser on the surface of the welding seam after root pass welding. It can be found that the two images are different in a very large degree. So they should be dealt with different strategies. The method proposed in Section 4 is difficult to deal with the image as given in Fig. 7(b). However, the two im-

ages have a common property, that is, the area of the welding seam is just part of the image. So the welding seam area should be detected to reduce the computation cost (Li et al., 2005).

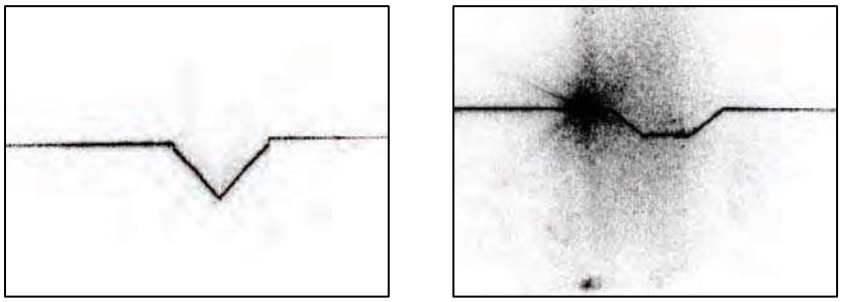

(a) (b)

Figure 7. Images of welding seams before and after root pass welding

5.1.1 Welding seam area detection

In order to reduce the computational time required in image processing, only the image of welding seam area is processed. However, some disturbances such as reflection shown in Fig. 7(b) will be segmented in the object area with the method in Section 4, which increases the difficulty of features extraction later. Here, an intensity distribution method is presented to detect the object area. The laser stripes shown in Fig. 7, captured by another visual sensor, are horizontal; their range in column is almost from the first to end. So only the range in row needs to be detected. It can be determined by calculating the distribution of intensity of pixels in row. Apparently, the main peak of intensity is nearby to the position of the main vector of laser stripe. So the range of seams in *Y*-axis direction of the image plane can be detected reliably with (31).

$$\begin{cases} Y_2 = Min\{Y_p + h_w + m_w,\ n_h\} \\ Y_1 = Max\{Y_p - m_w,\ 0\} \end{cases} \tag{31}$$

where Y_p is the Y-coordinate of main vector; h_w is the height of welding groove; and m_w is the margin remained. The target area consists of 0, n_w, Y_1 and Y_2.

5.1.2 Column based processing

Column based profiles extraction calculates the distribution of pixels' intensity with columns to get the points of profile. Some algorithms such as multi-peak method and centre of gravity (Haug & Pristrchow, 1998), gradient detection and average of upper edges and the lower edges in Section 4 are all effective

for the task. In order to get high quality profiles of seams, a method that combines smoothing filter, maximum detection and neighbourhood criteria is proposed.

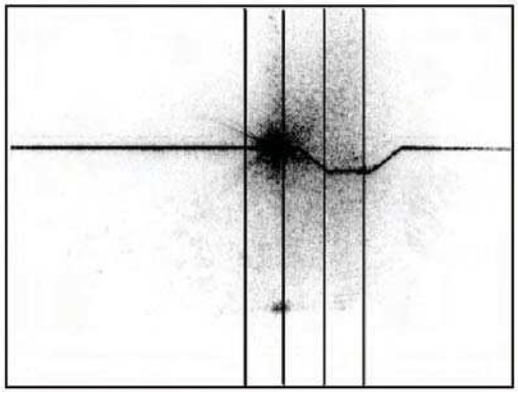

(a)

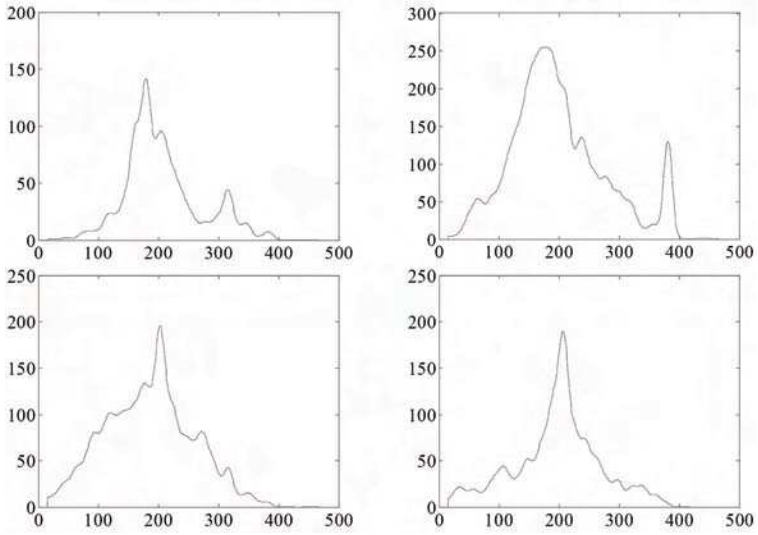

(b)

Figure 8. Intensity extraction of four columns

Firstly, a low pass filter is designed to smooth the intensity curve of column *i*. Usually, the pixels of profiles are in the area of main peak, and the peaks caused by disturbances are lower or thinner. After smoothing the intensity curve, the plateau is smoothed with one maximum in main peak, and the lower or thinner peaks are smoothed into hypo-peaks. Fig. 8 gives an example of intensity distribution of column 300, 350, 400, 450 of a welding seam image. Fig. 8(a) shows the original image and the positions of four example columns. Fig. 8(b) shows their intensity distribution.

Then according to the analysis of the image gray frequency, the self-adaptive thresholds of the images are calculated. Only the pixels whose intensity exceeds the thresholds are regards as valid. Thus the intensity curve is fragmented to several peaks. By calculating the area of peaks, the main peak can be gotten.
In this way, there is only one point with maximum intensity remained on the main peak in the intensity distribution curve. In other words, one point on the profile for each column is detected. Thus an array of points indexed with column is extracted through intensity distribution from the welding image.
In order to extract points of profile more properly, the criterion of neighbour is applied. Since the profiles of grooves should be a continuous curve, the points that are apparently inconsistent to neighbour points should be rejected. When the pixels whose intensity value exceeds the thresholds cannot be found, there will be no record in the array for this column. In these situations, the data in the array will be not continuous. Then the linear interpolation algorithm is used to fill up the curve between broken points, and the discrete points array is transferred to continuous profile curve.

5.2 Features extraction for seam tracking

In order to extract features of profiles for seam tracking, the first task is to select features. Usually the corner points of profiles are brim points of the welding groove, and they are often selected as features of welding seams in single pass welding (Kim et al., 1996; Wu et al., 1996). The corner detection method is only valid for images of single pass welding. But in multi-pass welding, there is distortion caused by weld bead in the bottom of groove. There are welding slag remained on the surface of welding work piece sometimes. As shown in Fig. 7(b), it is hard to judge the proper corner points by the second derivative because of the distortion. So the features extraction with corner point's detection is not reliable in this case.
The centre of gravity of groove area is selected as features because of its good stabilization relative to corner points.
Fig. 9(a) shows a profile of groove extracted with the method in Section 5.1 from a welding seam after welding root pass. Firstly, the profile is smoothed by a Hanning filter to eliminate high frequency noise, as shown in Fig. 9(b). In order to get the figure of groove area, the main vector of the profile is required. It can be extracted by Hough transform as described in Section 4.
Because the main vector is the asymptote of the profile, the main vector and the profile can form a trapeziform figure approximately. In the first step, the bottom of groove area is detected by template matching. Then from the bottom of groove, the points on the profile are searched forward and backward respectively.

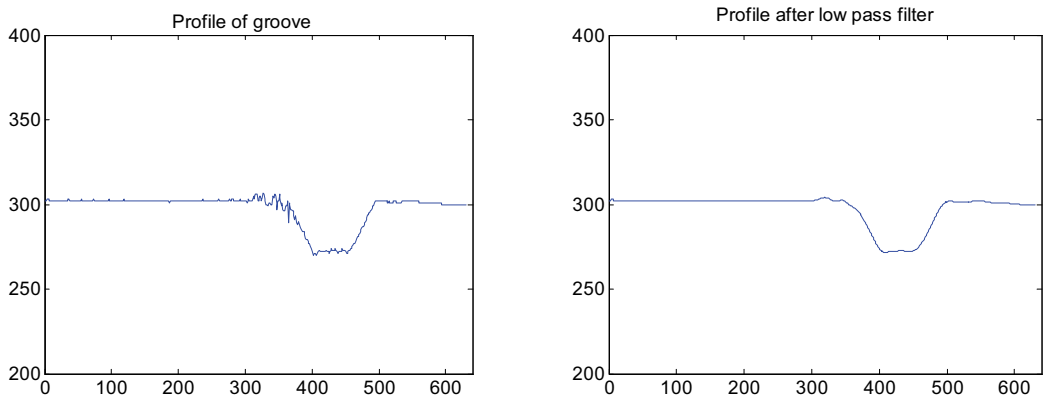

Figure 9. Profiles of the groove after root pass

The two borders (b1, b2) of the figure are gotten when the distances between the points on the profile and the main vector are less than the thresholds (5 pixels here). The trapeziform figure is defined with the border points, as shown in Fig. 10. Finally, the gravity centre of the figure is extracted as features by (32). A perpendicular to the main vector is drawn through the gravity centre. The intersection is taken as the feature point of the welding seam.

$$\begin{cases} F_u = \sum_{i=b1}^{b2} i\left[y_p(i) - y_v(i)\right] \Big/ \sum_{i=b1}^{b2} \left[y_p(i) - y_v(i)\right] \\ F_v = \sum_{i=b1}^{b2} 0.5\left[y_p(i)^2 - y_v(i)^2\right] \Big/ \sum_{i=b1}^{b2} \left[y_p(i) - y_v(i)\right] \end{cases} \tag{32}$$

where F_u, F_v are the coordinates of geometric centre; y_p and y_v are Y-coordinates of points on the profile and the main vector.

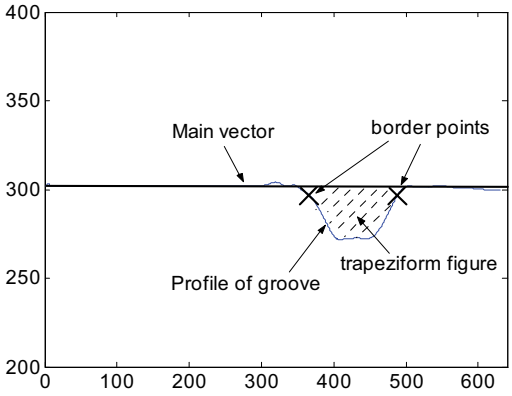

Figure 10. Main vector and border points on the groove profile

6. Hybrid visual control method for robotic welding

6.1 Jacobian matrix from the image space to the Cartesian space of the end-effector

From (3) and (4), formula (33) is deduced (Xu et al., 2004b; 2005).

$$\begin{bmatrix} x_c \\ y_c \\ z_c \end{bmatrix} = -\left(\begin{bmatrix} a & b & c \end{bmatrix} \begin{bmatrix} x_{c1} \\ y_{c1} \\ 1 \end{bmatrix} \right)^{-1} \begin{bmatrix} x_{c1} \\ y_{c1} \\ 1 \end{bmatrix} \tag{33}$$

Further more, the coordinates of a point P in Cartesian space are obtained as (34) in the end-effector frame.

$$\begin{bmatrix} x_e \\ y_e \\ z_e \\ 1 \end{bmatrix} = {}^{e}M_c \begin{bmatrix} x_c \\ y_c \\ z_c \\ 1 \end{bmatrix} = \begin{bmatrix} {}^{e}m_{xc} & {}^{e}n_{xc} & {}^{e}o_{xc} & {}^{e}p_{xc} \\ {}^{e}m_{yc} & {}^{e}n_{yc} & {}^{e}o_{yc} & {}^{e}p_{yc} \\ {}^{e}m_{zc} & {}^{e}n_{zc} & {}^{e}o_{zc} & {}^{e}p_{zc} \\ 0 & 0 & 0 & 1 \end{bmatrix} \begin{bmatrix} x_c \\ y_c \\ z_c \\ 1 \end{bmatrix} = \begin{bmatrix} {}^{e}R_c & {}^{e}p_c \\ 0 & 1 \end{bmatrix} \begin{bmatrix} x_c \\ y_c \\ z_c \\ 1 \end{bmatrix} \tag{34}$$

in which, ${}^{e}M_c$ is the extrinsic parameter matrix of the camera relative to the end-effector of the robot. ${}^{e}R_c$ is the rotation translation matrix, and ${}^{e}p_c$ is the position vector.

The time derivative of (34) is as follows.

$$\begin{bmatrix} \dot{x}_e \\ \dot{y}_e \\ \dot{z}_e \\ 0 \end{bmatrix} = \begin{bmatrix} {}^{e}R_c & {}^{e}p_c \\ 0 & 1 \end{bmatrix} \begin{bmatrix} \dot{x}_c \\ \dot{y}_c \\ \dot{z}_c \\ 0 \end{bmatrix} \Rightarrow \begin{bmatrix} \dot{x}_e \\ \dot{y}_e \\ \dot{z}_e \end{bmatrix} = {}^{e}R_c \begin{bmatrix} \dot{x}_c \\ \dot{y}_c \\ \dot{z}_c \end{bmatrix} \tag{35}$$

Submitting (5) into (33) and applying time derivative, then (Xu et al., 2005)

$$\begin{aligned} \begin{bmatrix} \dot{x}_c \\ \dot{y}_c \\ \dot{z}_c \end{bmatrix} &= \frac{1}{D^2} \begin{bmatrix} -b(v-v_0)/(k_x k_y) - c/k_x & b(u-u_0)/(k_x k_y) & 0 \\ a(v-v_0)/(k_x k_y) & -a(u-u_0)/(k_x k_y) - c/k_y & 0 \\ a/k_x & b/k_y & 0 \end{bmatrix} \begin{bmatrix} \dot{u} \\ \dot{v} \\ 0 \end{bmatrix} \\ &= \frac{1}{D^2} \begin{bmatrix} -b(v-v_0)/(k_x k_y) - c/k_x & b(u-u_0)/(k_x k_y) \\ a(v-v_0)/(k_x k_y) & -a(u-u_0)/(k_x k_y) - c/k_y \\ a/k_x & b/k_y \end{bmatrix} \begin{bmatrix} \dot{u} \\ \dot{v} \end{bmatrix} = J_c(u,v) \begin{bmatrix} \dot{u} \\ \dot{v} \end{bmatrix} \end{aligned} \tag{36}$$

in which, $J_c(u,v)$ is the Jacobian matrix from image space to Cartesian space in the camera frame *C*. $D = a(u-u_0)/k_x + b(v-v_0)/k_y + c$, is a constraint of the laser plane.
Submitting (36) to (35), the Jacobian matrix from image space to Cartesian space in the end-effector frame *E* is obtained, as given in (37).

$$\begin{bmatrix} \dot{x}_e \\ \dot{y}_e \\ \dot{z}_e \end{bmatrix} = J(u,v)\begin{bmatrix} \dot{u} \\ \dot{v} \end{bmatrix} \Rightarrow \begin{bmatrix} dx_e \\ dy_e \\ dz_e \end{bmatrix} = J(u,v)\begin{bmatrix} du \\ dv \end{bmatrix} \tag{37}$$

where symbol *d* represents derivative.
Formula (38) gives the Jacobian matrix from image space to Cartesian space in the end-effector frame, which describes the relation of the differential movements between a feature point on image plane and the end-effector. The parameters in (38), such as [k_x, k_y], [u_0, v_0], ${}^eR_c$, *a*, *b* and *c*, can be achieved through camera and laser plane calibration.

$$J(u,v) = {}^eR_c J_c(u,v) = \frac{1}{D^2}\,{}^eR_c \begin{bmatrix} -b(v-v_0)/(k_x k_y) - c/k_x & b(u-u_0)/(k_x k_y) \\ a(v-v_0)/(k_x k_y) & -a(u-u_0)/(k_x k_y) - c/k_y \\ a/k_x & b/k_y \end{bmatrix} \tag{38}$$

6.2 Hybrid visual servoing control

6.2.1 The model of hybrid visual servoing control for robotic arc welding

The scheme of hybrid visual servoing control method proposed in this chapter for robotic arc welding consists of four main parts, such as the control of moving along welding seam, the control of tracking adjusting, the position control of the robot, and the image feature extraction. The block diagram is shown in Fig. 11. Position-based visual control in Cartesian space is employed in the process of moving along the welding seam. From the image of the structured light stripe at *i*-th sampling, the image coordinates u_i' and v_i' for feature point P_i on the stripe can be extracted. Then [x_{ei}, y_{ei}, z_{ei}], the coordinates of point P_i in the end-effector frame, can be computed with (5), (33) and (34). In addition, the coordinates of point P_{i-1} in the current end-effector frame, [x_{ei-1}, y_{ei-1}, z_{ei-1}], can be obtained through transformation according to the movement Δ_i of the end-effector at last times. Then the direction of welding seam is determined with [x_{ei-1}, y_{ei-1}, z_{ei-1}] and [x_{ei}, y_{ei}, z_{ei}]. For reducing the influence of random ingredients, the coordinates of n+1 points P_{i-n}-P_i in the end-effector frame can be used to calculate the direction of the welding seam through fitting. The direction

vector of the welding seam is taken as movement Δ_{li} of the end-effector after multiplying with a proportion factor K. In the part of the control of moving along welding seam, the measured direction above is taken as the desired value to control the movement of the robot. It is inevitable that there exist apparent errors in the process of moving along the welding seam. Therefore the second part, that is, tracking adjusting with visual servoing control in image space, is introduced. According to the desired image coordinates $[u, v]$ and the actual ones $[u_i', v_i']$ of the feature point P_i, the errors $[du_i, dv_i]$ of the image coordinates as well as the estimated Jacobian matrix $\hat{J}(u,v)$ are calculated. Then $[d\hat{x}_e, d\hat{y}_e, d\hat{z}_e]$ is computed using (37), which is considered as the position errors of the end-effector. The differential movement Δ_{si} of the end-effect-or is generated with PID algorithm according to these errors. Δ_i, the sum of Δ_{si} and Δ_{li}, is taken as the total movement of the end-effector. The third part, the position control of the robot, controls the motion of the robot according to Δ_i. In detail, the position and pose of the end-effector in next step, in the world frame, is calculated with the current one and Δ_i. The joint angle value for each joint of the robot is calculated using inverse kinematics from the position and pose of the end-effector in next step. Then the position controller for each joint controls its motion according to the joint angle. The position control of the robot is realized with the control device attached to the robot set.

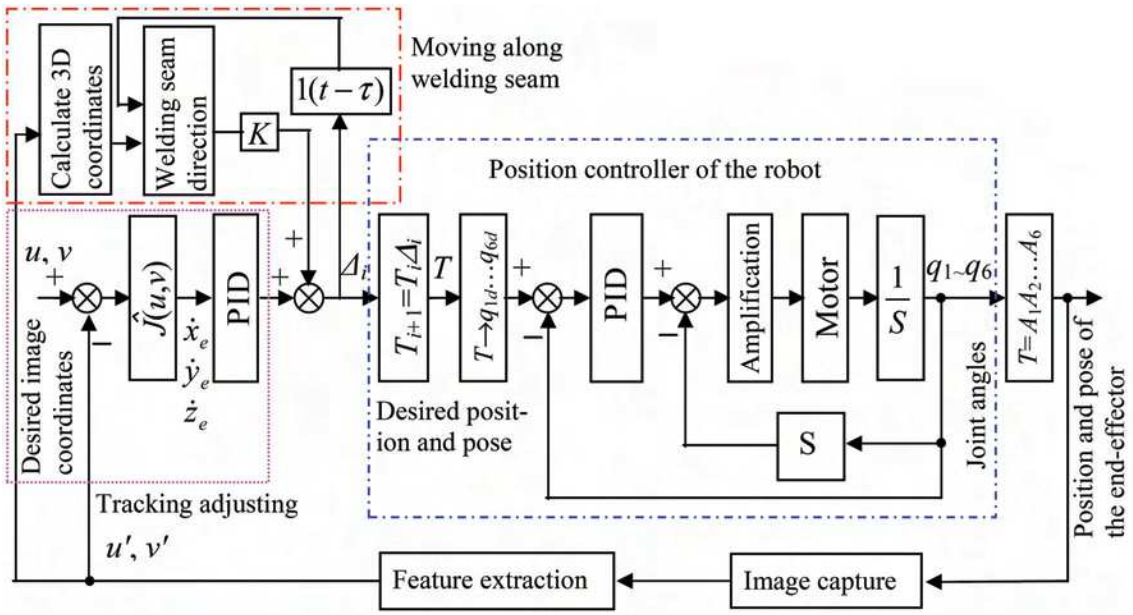

Figure 11. The block diagram of hybrid visual servoing control for robotic arc welding

The other parts such as the control of moving along welding seam, tracking adjusting and image feature extraction are completed with an additional computer (Xu et al., 2005).

6.2.2 The model simplification

In the hybrid visual servoing control system for robotic arc welding, as shown in Fig. 11, the control of moving along welding seam takes the direction of welding seam as the desired value to make the end-effector to move ahead. Its output Δ_{li} can be considered as disturbance $\xi(t)$ for the part of image-based visual servoing control. In the part of the position control of the robot, the motions of the robot are merely controlled according to the desired movements of the end-effector and the stated velocity. In the condition that the movement velocity is low, the part of the position control for the movement of the end-effector can be considered as a one-order inertia object. Therefore, the model of the hybrid visual servoing control system can be simplified to the dynamic framework as shown in Fig. 12.

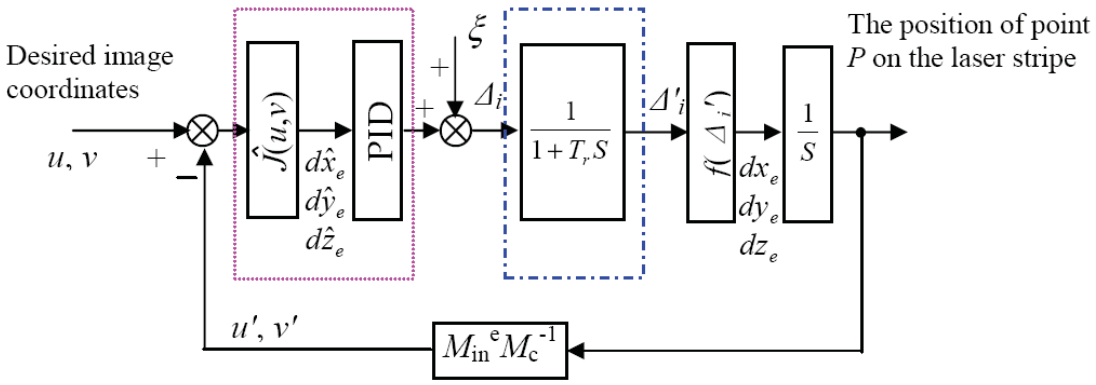

Figure 12. The simplified block diagram of hybrid visual servoing control for robotic arc welding

Although the laser stripe moves with the end-effector, the position $[x_e, y_e, z_e]$, in the end-effector frame, of the feature point P on the stripe will vary with the movement of the end-effector. The relation between the movement of the end-effector and $[x_e, y_e, z_e]$ is indicated as $f(\Delta_i')$. The model for the camera and image capture card is described as $M_{in}{}^{e}M_c^{-1}$.

6.2.3 The relation between the end-effector's movement and the feature point position

In the end-effector frame, the equation of the laser plane can be expressed as (39).

$$\begin{cases} a_e x + b_e y + c_e z + 1 - d_e = 0 \\ a_e = am_x + bn_x + co_x \\ b_e = am_y + bn_y + co_y \\ c_e = am_z + bn_z + co_z \\ d_e = a\vec{m}\cdot\vec{p} + b\vec{n}\cdot\vec{p} + c\vec{o}\cdot\vec{p} \end{cases} \tag{39}$$

where $\vec{m} = \begin{bmatrix} m_x & m_y & m_z \end{bmatrix}^T$, $\vec{n} = \begin{bmatrix} n_x & n_y & n_z \end{bmatrix}^T$, and $\vec{o} = \begin{bmatrix} o_x & o_y & o_z \end{bmatrix}^T$ are the orientation vector of ${}^{e}M_{c}$ as (34).

Assume the equation of the welding seam, in the end-effector frame, at the i-th sampling is as given in (40).

$$\begin{cases} x_{li} = x_{li0} + k_x t \\ y_{li} = y_{li0} + k_y t \\ z_{li} = z_{li0} + k_z t \end{cases} \tag{40}$$

From (39) and (40), the coordinates of the feature point P_i on the stripe, in the end-effector frame, at the i-th sampling is deduced, seen in (41).

$$\begin{cases} x_{ei} = x_{li0} + k_x t_i \\ y_{ei} = y_{li0} + k_y t_i \\ z_{ei} = z_{li0} + k_z t_i \\ t_i = \dfrac{d_e - 1 - a_e x_{li0} - b_e y_{li0} - c_e z_{li0}}{a_e k_x + b_e k_y + c_e k_z} \end{cases} \tag{41}$$

After the movement of the end-effector $\Delta_i' = [\Delta'_{ix}, \Delta'_{iy}, \Delta'_{iz}]^T$, the equation of the welding seam in the end-effector frame is obtained.

$$\begin{cases} x_{li+1} = x_{li0} + \Delta'_{ix} + k_x t \\ y_{li+1} = y_{li0} + \Delta'_{iy} + k_y t \\ z_{li+1} = z_{li0} + \Delta'_{iz} + k_z t \end{cases} \tag{42}$$

Applying (42) to (39), the resolution obtained as (43) is the coordinates of the feature point P_{i+1} on the stripe, in the end-effector frame, at the i+1-th sampling.

$$\begin{cases} x_{ei+1} = x_{li0} + \Delta'_{ix} + k_x t_{i+1} \\ y_{ei+1} = y_{li0} + \Delta'_{iy} + k_y t_{i+1} \\ z_{ei+1} = z_{li0} + \Delta'_{iz} + k_z t_{i+1} \\ t_{i+1} = \dfrac{d_e - 1 - a_e(x_{li0} + \Delta'_{ix}) - b_e(y_{li0} + \Delta'_{iy}) - c_e(z_{li0} + \Delta'_{iz})}{a_e k_x + b_e k_y + c_e k_z} \end{cases} \tag{43}$$

By comparing (41) and (43), the relation of the coordinates between P_{i+1} and P_i in the end-effector frame is derived.

$$\begin{cases} x_{ei+1} = x_{ei} + \Delta'_{ix} + k_x t_{ii+1} \\ y_{ei+1} = y_{ei} + \Delta'_{iy} + k_y t_{ii+1} \\ z_{ei+1} = z_{ei} + \Delta'_{iz} + k_z t_{ii+1} \\ t_{ii+1} = \dfrac{-a_e \Delta'_{ix} - b_e \Delta'_{iy} - c_e \Delta'_{iz}}{a_e k_x + b_e k_y + c_e k_z} \end{cases} \tag{44}$$

Formula (44) can be rewritten in the form of matrix as (45).

$$\begin{bmatrix} dx_{ei+1} \\ dy_{ei+1} \\ dz_{ei+1} \end{bmatrix} = \begin{bmatrix} x_{ei+1} - x_{ei} \\ y_{ei+1} - y_{ei} \\ z_{ei+1} - z_{ei} \end{bmatrix} = \begin{bmatrix} 1 - a_e k_x / D_e & -b_e k_x / D_e & -c_e k_x / D_e \\ -a_e k_y / D_e & 1 - b_e k_y / D_e & -c_e k_y / D_e \\ -a_e k_z / D_e & -b_e k_z / D_e & 1 - c_e k_z / D_e \end{bmatrix} \begin{bmatrix} \Delta'_{ix} \\ \Delta'_{iy} \\ \Delta'_{iz} \end{bmatrix} = F \begin{bmatrix} \Delta'_{ix} \\ \Delta'_{iy} \\ \Delta'_{iz} \end{bmatrix} \tag{45}$$

where $D_e = a_e k_x + b_e k_y + c_e k_z$ represents the constraint of the equation of the structured light plane in the end-effector frame. D_e is a constant for line shaped welding seams with the movement of robot. F is a transformation matrix, which describes the relation of the position variations between the end-effector and the feature point P on the stripe in the end-effector frame.

6.2.4 Stability analysis

Suppose the error vector $\vec{e} = [du \quad dv]^T = [u - u' \quad v - v']^T$. The states variables are selected as $X_1 = \vec{e}$, $X_2 = \Delta_i = [\Delta_{ix} \quad \Delta_{iy} \quad \Delta_{iz}]^T$, and $X_3 = \Delta'_i = [\Delta'_{ix} \quad \Delta'_{iy} \quad \Delta'_{iz}]^T$. It is easy to establish the state equation of the system as (46) reference from Fig. 12.

$$\begin{cases} \dot{X}_1 = -M_{in}\ {}^e M_c^{-1} F X_3 \\ \dot{X}_2 = K_i \hat{J} X_1 - (1/T_r) K_d \hat{J} M_{in}\ {}^e M_c^{-1} F X_2 + (K_d / T_r - K_p) \hat{J} M_{in}\ {}^e M_c^{-1} F X_3 \\ \dot{X}_3 = (1/T_r) X_2 - (1/T_r) X_3 \end{cases} \tag{46}$$

A positive Lyapunov function V is configured as (47). Its time derivative is seen in (48).

$$V = \frac{1}{2}(\hat{J}X_1)^T \hat{J}X_1 + \frac{1}{2}X_2{}^T X_2 + \frac{1}{2}X_3{}^T X_3 \tag{47}$$

$$\begin{aligned}
\dot{V} &= -(\hat{J}X_1)^T \hat{J}M_{in}\ {}^eM_c^{-1}FX_3 + X_2^T K_i \hat{J}X_1 - \frac{1}{T_r}X_2^T K_d \hat{J}M_{in}\ {}^eM_c^{-1}FX_2 \\
&+ X_2^T[(\frac{1}{T_r}K_d - K_p)\hat{J}M_{in}\ {}^eM_c^{-1}F + \frac{1}{T_r}]X_3 - \frac{1}{T_r}X_3^T X_3 \\
&= -\frac{1}{2}(\hat{J}X_1)^T \hat{J}M_{in}\ {}^eM_c^{-1}F\hat{J}X_1 + \frac{1}{2}(\hat{J}X_1 - X_3)^T \hat{J}M_{in}\ {}^eM_c^{-1}F(\hat{J}X_1 - X_3) - \frac{1}{2}X_3^T \hat{J}M_{in}\ {}^eM_c^{-1}FX_3 \\
&+ \frac{1}{2}(\hat{J}X_1)^T K_i \hat{J}X_1 - \frac{1}{2}(\hat{J}X_1 - X_2)^T K_i(\hat{J}X_1 - X_2) + \frac{1}{2}X_2^T K_i X_2 - \frac{1}{T_r}X_2^T K_d \hat{J}M_{in}\ {}^eM_c^{-1}FX_2 \\
&+ \frac{1}{2}X_2^T[(\frac{1}{T_r}K_d - K_p)\hat{J}M_{in}\ {}^eM_c^{-1}F + \frac{1}{T_r}]X_2 + \frac{1}{2}X_3^T[(\frac{1}{T_r}K_d - K_p)\hat{J}M_{in}\ {}^eM_c^{-1}F + \frac{1}{T_r}]X_3 \\
&- \frac{1}{2}(X_2 - X_3)^T[(\frac{1}{T_r}K_d - K_p)\hat{J}M_{in}\ {}^eM_c^{-1}F + \frac{1}{T_r}](X_2 - X_3) - \frac{1}{T_r}X_3^T X_3 \\
&\le -\frac{1}{2}(\hat{J}X_1)^T(\hat{J}M_{in}\ {}^eM_c^{-1}F - K_i)\hat{J}X_1 - \frac{1}{2}X_2^T(K_p\hat{J}M_{in}\ {}^eM_c^{-1}F - \frac{I}{T_r} - K_i)X_2 \\
&- \frac{1}{2}X_3^T(I + K_p - \frac{1}{T_r}K_d)\hat{J}M_{in}\ {}^eM_c^{-1}FX_3 + o(\delta^2)
\end{aligned} \tag{48}$$

where I is a unit matrix, and $o(\delta^2) = \frac{1}{2}(\hat{J}X_1 - X_3)^T \hat{J}M_{in}\ {}^eM_c^{-1}F(\hat{J}X_1 - X_3)$ is a two-order infinitely small quantity term that can be ignored.

Obviously, if the condition (49) is satisfied, then $\dot{V} < 0$. According to the stability theorem of Lyapunov, the system is asymptotic stable.

$$\begin{cases}
K_i < \hat{J}M_{in}\ {}^eM_c^{-1}F \\
K_i < K_p\hat{J}M_{in}\ {}^eM_c^{-1}F - \dfrac{I}{T_r} \\
K_d < T_r I + T_r K_p
\end{cases} \tag{49}$$

Discussion: (1) As the ideal case, the parameters of the camera and the laser plane are accurately calibrated, that is, $\hat{J} = J$. It is easy to validate that $\hat{J}M_{in}\ {}^eM_c^{-1}F = I$ is satisfied. It means that the system is degenerated as a linear system.

(2) In the case that there exist errors in $\hat{J}$, if $\hat{J}M_{in}\ {}^eM_c^{-1}F$ is positive definite, then the PID parameters that satisfy condition (49) can make the system be asymptotic stable.

(3) If $\hat{J}M_{in}\ {}^eM_c^{-1}F$ is negative definite, then it is not ensured that the system is stable.

6.3 Experiment and results

The experiment system consists of a master computer, a local controller of the robot, a robot Yaskawa UP6, a camera, a laser emitter, welding power source, a welding wire supplier, a welding gun and a CO_2 gas container. The master computer is for image features extraction, the control of moving along welding seam, and the control of tracking adjusting. It outputs the relative movement value Δ_i of the end-effector to the local controller of the robot. The local controller controls the robot to move according to Δ_i. The camera, laser emitter and the welding gun are all fixed on the end-effector of the robot. The stripe formed by the laser plane projecting on the welding seam is ahead of the welding gun tip about 25mm.

Firstly, the camera and the laser plane were calibrated. The intrinsic parameters and extrinsic ones relative to the end-effector frame are as follows. Here, the image size was 768×576 in pixel.

$$M_{in}=\begin{bmatrix}2663.8 & 0 & 445.7\\ 0 & 2655.9 & 321.0\\ 0 & 0 & 1\end{bmatrix},\ {}^{e}M_{c}=\begin{bmatrix}-0.1301 & -0.6102 & -0.7815 & 54.5258\\ -0.0299 & 0.7903 & -0.6120 & -87.5896\\ 0.9911 & -0.0562 & -0.1210 & 39.1279\\ 0 & 0 & 0 & 1\end{bmatrix}$$

The laser plane equation in the camera frame is: $-0.000862x+0.004382y-0.004470z+1=0$.

It is a key factor of the visual control to select stable image features. Aiming at the structured light images as shown in Fig. 5, the points with local maximum slope variation in the stripe was selected as candidate feature points. The obvious advantage of our strategy was that the feature points selected above are on the centre line of the welding seam, such as a type V groove welding seam and a lap one. The image processing and feature extraction method in Section 4 was employed to compute the image coordinates of the feature points. The position and pose of the welding gun was adjusted adequately before welding. The images captured at this time were free from the arc light. The image coordinates of the feature point could be extracted more accurately. They were taken as the desired image coordinates $[u, v]$ for the part of tracking adjusting control. During welding, multiple candidate feature points may be obtained sometimes. In this case, the candidate feature point which image coordinates are nearest to $[u, v]$ is selected as feature point.

In the experiment of tracking and welding, the moving velocity of the robot was set to 0.003m/s. The PID parameters in tracking adjusting control were given as:

$$K_p = \begin{bmatrix} 0.5 & 0 & 0 \\ 0 & 0.5 & 0 \\ 0 & 0 & 0.5 \end{bmatrix}, K_d = 0, K_i = \begin{bmatrix} 0.05 & 0 & 0 \\ 0 & 0.01 & 0 \\ 0 & 0 & 0.02 \end{bmatrix}$$

The experimental welding seams were a type V groove welding seam and a lap one. The protection gas was CO_2. The transition mode of welding was short circuit. The welding experiments for a type V groove welding seam and a lap one were respectively conducted by using the methods proposed in this chapter. The results showed that the welding seam could be recognized and tracked well. And the shape of weld mark was good. Fig. 13 shows the results of welding experiment for a lap welding seam. The situation for pixel coordinate u' of feature point during tracking and welding is shown in Fig. 13(a), and v' in Fig. 13(b). Their horizontal coordinates are sample times. The pixel coordinates $[u', v']$ of feature points during tracking and welding are shown in Fig. 13(c). The weld mark after welding is in Fig. 13(d). It can be found that there existed larger errors near by the end stage. It was because of a small piece of scrap on the welding seam, which resulted in the image coordinates of the feature point with large errors.

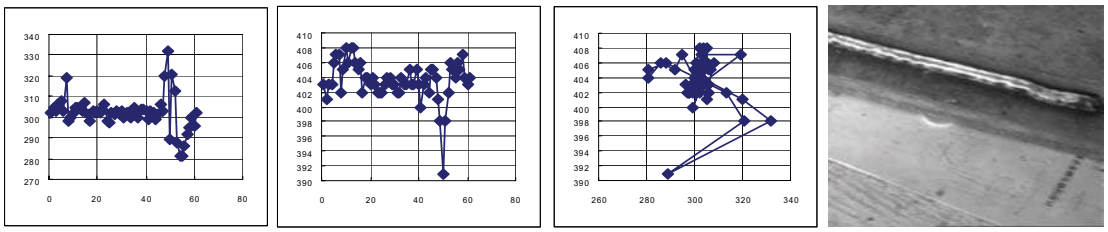

(a) (b) (c) (d)

Figure 13. The experimental results

7. Conclusions

A visual control system for robotic welding is introduced in this chapter. The calibration of a vision sensor, the processing algorithms for laser stripe images, and a hybrid visual control method are discussed in detail.

Based on the robot's movement, a method of the structured light vision sensor's calibration is proposed. The laser plane can be calibrated from a group of rotation movements. The experimental results show its effectiveness. It is easy to be realized and provides the possibility to run hand-eye system calibration automatically.

The image processing algorithms proposed in this chapter include two catego-

ries such as feature extraction methods based on second order difference and geometric centre. The former can recognize welding seam of type V groove and find feature points with precise in the case of strong reflection, arc light and splash disturbance. The latter can robustly provide feature points for the welding seam after root pass welding.

A hybrid visual servoing method is proposed in this chapter, which consists of a position control inner-loop in Cartesian space and two outer-loops. One is position-based visual control in Cartesian space; another is image-based visual servoing control in image space. The former is employed for the control of moving along the direction of the welding seam. The latter is for the control of tracking adjusting. The Jacobian matrix from image space of the feature point on structured light stripe to Cartesian space is variable with the movement of the end-effector. But there exists not singular problem in the Jacobian matrix. So the target can be kept in the view field of the camera with the control method above. In the case that the errors between the estimated and real parameters of the camera and the laser plane are not very large, the asymptotic stability of the control system can be ensured through the selection of adequate PID parameters.

The experimental results show the effectiveness of the hybrid visual servoing control system for robotic arc welding. The current position and pose are not necessary for the hybrid visual servoing control system. So it can be applied to many kinds of robots, which can accept the commands of relative movement to the end-effector, to realize visual measurement and tracking.

In addition, whether the work piece is clean or not has obvious influence on the visual measurement results. The unclean surface sometimes results in gross errors of the welding seam tracking. How to eliminate the influence of the gross errors in image space is our work in near future. And the automated adjustment of the position and pose of the welding gun in the start stage is another problem to deal with in future.

Acknowledgement

The authors would like to thank the National High Technology Research and Development Program of China for the support to this work under grant No.2002AA422160. We would also like to thank like to thank National Key Fundamental Research and Development Project of China (973, No.2002CB312200) for the support to this work.

8. References

Bakos, G. C.; Tsagas, N. F.; Lygouras, J. N.; Lucas J. (1993). Long distance non-contact high precision measurements. *International Journal of Electronics*, Vol. 75, No. 6, pp. 1269-1279, ISSN: 0020-7217.

Bolmsjo, G.; Olsson, M. & Cederberg, P. (2002). Robotic arc welding—trends and developments for higher autonomy. *The Industrial Robot*, Vol. 29, No. 2, pp. 98-104, ISSN: 0143-991X.

Cervera, E.; Berry, F. & Martinet, P. (2002). Image-based stereo visual servoing: 2D vs 3D features. *15th Triennial World Congress of the International Federation of Automatic Control*, pp. 1630-1635, ISBN: 0-08-044295-1, Barcelona, Spain, July 2002, Elsevier Science Press.

Chaumette, F. & Malis, E. (2000). 2 1/2 D visual servoing: a possible solution to improve image-based and position-based visual servoings. *IEEE International Conference on Robotics and Automation*, pp. 630-635, ISBN: 0-7803-5889-9, San Francisco, USA, Apr. 2000, Institute of Electrical and Electronics Engineers Inc., Piscataway, USA

Corke, P. I. & Good, M. C. (1993). Controller design for high-performance visual servoing. *Proceedings 12th World Congress International Federation of Automatic Control*, Vol. 9, pp. 395-398, ISBN: 0-08-042211-X, Sydney, Australia, July 1993, Elsevier Science Press.

Corke, P. I. & Good, M. C. (1996). Dynamic effects in visual closed-loop systems. *IEEE Transaction on Robotics and Automation*, Vol. 12, No. 5, pp. 671-683, ISSN: 1042-296X.

Faugeras, O. D. & Toscani, G. (1986). The calibration problem for stereo. *IEEE Computer Society Conference on Computer Vision and Pattern Recognition*, pp. 15-20, ISBN: 0-8186-0721-1, Miami Beach, USA, 1986, IEEE Press, New York, USA.

Hager, G. D.; Hutchinson, S. & Corke, P. I. (1996). A tutorial on visual servo control. *IEEE Transaction on Robotics and Automation*, Vol. 12, No. 5, pp. 651-670, ISSN: 1042-296X.

Haug, K. & Pristrchow, G. (1998). Robust laser stripe sensor for the automated welding seam tracking in the shipbuilding industry. *Proceedings of the 24th Annual Confer-ence of the IEEE Industry Electronics Society*, pp. 1236-1241, Aachen, Germany, Sep. 1998, IEEE Comp Soc, Los Alamitos, USA.

Kim, J. S.; Son, Y. T.; Cho, H. S.; Koh, K. I. (1996). A robust visual seam tracking system for robotic arc welding. *Mechantronics*, Vol. 6, No. 2, pp. 141-163, ISSN: 0957-4158.

Li, Y.; Xu, D. & Tan, M. (2005). Robust features extraction for structured light images of welding seam in multi-pass submerged arc welding, *7th International Conference on Electronic Measurement & Instruments*, Vol. 6, pp. 1559-1563, ISBN: 7-5062-7443-4, Beijing, China, Aug. 2005, International Academic Publishers, Beijing.

Ma, S. D. (1996). A self-calibration technique for active vision system. *IEEE Transaction on Robotics and Automation*, Vol. 12, No. 1, pp. 114-120, ISSN: 1042-296X.

Malis, E.; Chaumette, F. & Boudet, S. (1999). 2D 1/2 visual servoing. *IEEE Transaction on Robotics and Automation*, Vol. 15, No. 2, pp. 234-246, ISSN: 1042-296X.

Malis, E.; Chaumette, F. & Boudet, S. (1998). Positioning a coarse-calibrated camera with respect to an unknown object by 2D 1/2 visual servoing. *IEEE International Conference on Robotics and Automation*, Vol. 2, pp. 1352-1359, ISSN: 1050-4729, Leuven, Belgium, May 1998, IEEE Press, Piscataway, USA.

Tsai, R. Y. (1987). A versatile camera calibration technique for high-accuracy 3D machine vision metrology using off-the-shelf cameras and lens. *IEEE Transactions on Robotics and Automation*, Vol. 3, No. 4, pp. 323-344, ISSN: 1042-296X.

Wilson, M. (2002). The role of seam tracking in robotic welding and bonding. *Industrial Robot*, Vol. 29, No. 2, pp. 132-137, ISSN: 0143-991X.

Wu, J.; Smith, J. S. & Lucas, J. (1996). Weld bead placement system for multi-pass welding. *IEE Proceedings–Science, Measurement and Technology*, Vol. 143, No. 2, pp. 85-90, ISSN: 1350-2344.

Wu, L. & Chen, S. (2000). Intelligent technologies for welding, National Defence Indus-trial Press of China, ISBN: 7-118-02299-3, Beijing.

Xu, D.; Jiang, Z.; Wang, L. & Tan M. (2004a). Features extraction for structured light image of welding seam with arc and splash disturbance. *Proceedings of 8th International Conference on Control, Automation, Robotics and Vision*, pp. 1559-1563, ISBN: 0-7803-8653-1, Kunming, China, Dec. 2004, Institute of Electrical and Electronics Engineers Inc., New York, United States.

Xu, D.; Wang, L. & Tan, M. (2004b). Image processing and visual control method for arc welding robot, *IEEE International Conference on Robotics and Biomimetics*, pp. 727-732, ISBN: 0780386418, Shenyang, China, Aug. 2004, Institute of Electrical and Electronics Engineers Computer Society, Piscataway, United States.

Xu, D. & Tan, M. (2004). A calibration method for hand-eye system of arc welding robot, *10th IEEE International Conference on Methods and Models in Automation and Robotics*, pp. 903-908, ISBN: 83-88764-8, Miedzyzdroje, Poland, Aug. 2004, Institute of Control Engineering, Technical University of Szczecin, Szczecin, Poland.

Xu, D.; Wang, L.; Tu, Z. & Tan, M. (2005). Hybrid visual servoing control for robotic arc welding based on structured light vision, *Acta Automatica Sinica*, Vol. 31, No. 4, pp. 596-605, ISSN: 0254-4156.

Yoshimi, B. H. & Allen, P. K. (1994). Active uncalibrated visual servoing. *IEEE International Conference on Robotic & Automation*, Vol. 4, pp.156-161,

ISBN: 0-8186-5332-9, San Diego, USA, May 1994, IEEE Press, Piscataway, USA.

Zhang, J. & Djordjevich, A. (1999). Study on laser stripe sensor. *Sensors and Actuators A: Physical*, Vol. 72, No. 3, pp. 224-228, ISSN: 0924-4247.

Zhang, Z. (2000) A flexible new technique for camera calibration. *IEEE Transactions on Pattern Analysis and Machine Intelligence*, Vol. 22, No. 11, pp. 1330-1334, ISSN 0162-8828.

Zhu, S. & Qiang X. (2000). Analysis of 3-D coordinate vision measuring methods with feature points on workpiece. *Optics and Precision Engineering*, Vol. 8, No. 2, pp. 192-197, ISSN: 1004-924X.

Zou, D.; Ye, S. & Wang, C. (1995). Structured-lighting surface sensor and its calibration. *Optical Engineering*, Vol. 34, No. 10, pp. 3040-3043, ISSN: 0091-3286.

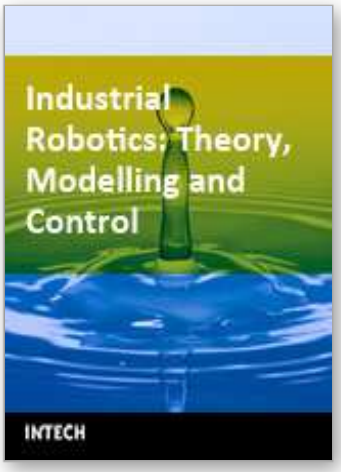

Industrial Robotics: Theory, Modelling and Control

Edited by Sam Cubero

ISBN 3-86611-285-8

Hard cover, 964 pages

Publisher Pro Literatur Verlag, Germany / ARS, Austria

Published online 01, December, 2006

Published in print edition December, 2006

This book covers a wide range of topics relating to advanced industrial robotics, sensors and automation technologies. Although being highly technical and complex in nature, the papers presented in this book represent some of the latest cutting edge technologies and advancements in industrial robotics technology. This book covers topics such as networking, properties of manipulators, forward and inverse robot arm kinematics, motion path-planning, machine vision and many other practical topics too numerous to list here. The authors and editor of this book wish to inspire people, especially young ones, to get involved with robotic and mechatronic engineering technology and to develop new and exciting practical applications, perhaps using the ideas and concepts presented herein.